Journal of Power Sources 439 (2019) 227073

Contents lists available at ScienceDirect

Journal of Power Sources

journal homepage: www.elsevier.com/locate/jpowsour

# A salt-derived solid electrolyte interphase by electroreduction of water-in-salt electrolyte for uniform lithium deposition

Zhenxing Wang [a,b,1], Chengguo Sun [c,1], Ying Shi [a], Fulai Qi [a], Qinwei Wei [a,b], Xin Li [a,b], Zhenhua Sun [a,b], Baigang An [c], Feng Li [a,b,c,*]

[a] Shenyang National Laboratory for Materials Science, Institute of Metal Research, Chinese Academy of Sciences, 72 Wenhua Road, Shenyang, 110016, China
[b] School of Materials Science and Engineering, University of Science and Technology of China, Hefei, 230026, China
[c] School of Chemical Engineering, University of Science and Technology Liaoning, Anshan, 114051, China

## HIGHLIGHTS

- The concept of salt-derived solid electrolyte interphase is proposed.
- This film is rich in inorganic components (mainly $Li_2S_xO_y$ and LiF).
- This film greatly reduces the overpotential and facilitates fast $Li^+$ transport.
- High Coulombic efficiency and uniform spherical Li deposition are achieved.
- This work emphasizes the functions of salt decompositions on protection of Li.

## ARTICLE INFO

*Keywords:*
Water-in-salt
Solid electrolyte interphase
Dendrite-free Li anode
Electroreduction
Space charge

## ABSTRACT

Notorious growth of dendritic lithium with low Coulombic efficiency causes safety and stability issues, which hinder practical applications. To control the lithium deposition so that one has a dendrite-free lithium metal anode with high Coulombic efficiency is highly desirable but challenging. Here, this work reports a copper substrate covered by a salt-derived solid electrolyte interphase that produced by electroreduction of a highly concentrated water-in-salt electrolyte to realize stable lithium deposition. Quite distinct from the resistive layer comprised principally of solvent-derived organic species (such as lithium alkyl carbonates) that produced in conventional dilute electrolyte, this salt-derived solid electrolyte interphase is rich in inorganic components (mainly $Li_2S_xO_y$ and LiF), which effectively reduce the overpotential and facilitate fast $Li^+$ transport. In addition, a small number of reduced fluorine organic anions -$CF_x$ stabilize the space charge to give a uniform distribution of $Li^+$. Such a solid electrolyte interphase on the copper substrate is able to modulate the lithium plating/stripping to produce uniform spherical lithium deposition with no dendrites, and a high Coulombic efficiency (≈98.2%) is achieved. This work provides a unique strategy to enlarge the functions of the lithium salt decompositions on the protection of lithium metal anodes.

## 1. Introduction

Lithium-ion batteries (LIBs) have achieved great success for use in portable devices and electric vehicles, but are unable to meet the currently ever-increasing demands of energy density [1]. The fact that the Li metal, with a specific capacity of an order of magnitude greater than that of the state-of-the-art $LiC_6$ anode, has attracted great interest in achieving rechargeable batteries with a higher energy density [2,3]. However, there is still a long way to go before the practical application of Li metal due to its poor safety, low Coulombic efficiency (CE) and short lifespan, its parasitic reactions with liquid electrolytes, and unstable and uncontrollable dendritic electrodeposition [4].

Such unsolved issues are associated with the high activity of Li metal. Li metal, which has the most negative electrochemical potential

* Corresponding author. Shenyang National Laboratory for Materials Science, Institute of Metal Research, Chinese Academy of Sciences, 72 Wenhua Road, Shenyang, 110016, China.
*E-mail address:* fli@imr.ac.cn (F. Li).
[1] These authors contributed equally to this work.

https://doi.org/10.1016/j.jpowsour.2019.227073
Received 1 March 2019; Received in revised form 3 July 2019; Accepted 26 August 2019
Available online 5 September 2019
0378-7753/© 2019 Elsevier B.V. All rights reserved.

(−3.04 V vs. a standard hydrogen electrode), can react spontaneously with all polar aprotic solvents [5,6]. When fresh Li metal is exposed to the electrolyte, an electrically insulating but ionically conducting solid electrolyte interphase (SEI) film is formed by parasitic reactions in milliseconds or less [7]. This film suppresses side-reactions by blocking electron transfer to produce passivation and protection of the active Li metal [8]. In a conventional dilute electrolyte for LIBs (usually 1 M Li salt dissolved in esters or ethers), the rational selection of solvents has been considered an effective route to passivate the negative electrodes. The passivated SEI film is principally comprised of RCOOLi, ROLi and ROCOLi (R: alkyl groups) etc., which greatly suppresses further reductive decomposition of the electrolyte [9]. In addition, small amounts of other inorganic products, including $Li_2CO_3$, $Li_2O$ and LiOH originating from the solvent or a Li salt, have been shown to be beneficial for stabilizing the SEI film [10]. In addition to passivating and stabilizing the Li metal, the SEI film plays a key role as a solid electrolyte for $Li^+$ transport [11]. However, ionic resistive species originating from the reduction of the organic solvents produce increased interfacial resistance and sluggish $Li^+$ transport, which cause nonhomogeneous Li deposition accompanied by dendrite formation [12]. To address the problem of nonhomogeneous Li deposition, much effort has been devoted to suppressing the growth of Li dendrites, including fluorinated interphases [13–15], electrolyte additives [16,17], a host [18–20], and an artificial protective layer [21,22]. Many studies have shown the important role of the SEI film in directing Li deposition/dissolution, so it is very important to design and tailor a high ion-conductivity, dense and homogeneous SEI film to achieve stable dendrite-free Li deposition.

In this work, we report a copper (Cu) substrate covered by a salt-derived SEI (donated as SDSEI) film that produced by electroreduction a highly concentrated water-in-salt electrolyte of lithium bis(trifluoromethane sulfonyl)imide (LiTFSI) to regulate Li plating/stripping. Rather than the resistive SEI layer comprised principally of solvent-derived organic ROLi species in conventional dilute electrolyte, this SDSEI film is rich in inorganic components (mainly $Li_2S_xO_y$ and LiF), which effectively reduces the overpotential and facilitates fast $Li^+$ transport. In addition, the presence of a small number of reduced fluorine organic anions (-$CF_x$), produces a uniform space charge distribution that contributes to homogeneous $Li^+$ deposition. Based on our modified Cu substrate, uniform deposition of spherical Li particles was obtained at different current densities. The Cu substrate with the SDSEI film allowed the achievement of a high CE of 98.2% over 140 cycles outperforming that of a bare Cu substrate in a half cell. A stable CE of ≈99.1% over 400 cycles in a Li-sulfur (Li–S) battery has great potential for practical use.

## 2. Materials and methods

### 2.1. Materials

Lithium bis(trifluoromethane sulfonyl)imide ($LiN(SO_2CF_3)_2$, LiTFSI) was purchased from Sigma-Aldrich. The aqueous water-in-salt electrolyte was made by dissolving 21 M LiTFSI (mol salt in kg solvent) in deionized water. Li metal foils (China Energy Lithium Co., Ltd) were used as received. Cu foils were bought from Shenzhen Kejing Technology Co., Ltd.

### 2.2. Preparation of the Cu substrate with the SDSEI film

To prepare the Cu substrate with the SDSEI film, bare Cu foil was first washed in ethanol and then acetone three times. Pre-processing was then performed in a three-electrode cell with a Cu foil as working electrode, Ag/AgCl in a saturated KCl aqueous solution as the reference electrode and glassy carbon as the counter electrode. The cyclic voltammetry measurements were performed in the range 1.9–3.2 V (vs. $Li^+$/Li) at a scan rate of 10 mV $s^{-1}$ for 100 cycles. The Cu substrate with the SDSEI film was washed in DME solvent to remove Li salt and then dried until the solvent had completely evaporated. The bare Cu substrate was processed at the same way except that the electrolyte was deionized water.

### 2.3. Electrochemical measurements

The Li | Cu cells were assembled or disassembled in an Ar-filled glove box with oxygen and water contents below 0.1 ppm. 2025-type coin cells were used to assemble Li | Cu cells and Li–S cells. For the Li | Cu cells, Li metal was used as the counter and reference electrode while the Cu substrate with the SDSEI film or bare Cu substrate were used as the working electrode. The Cu substrate with the SDSEI film or the bare Cu substrate was punched into a 16.0 mm diameter disk as the working electrode. The cells were cycled in the voltage range −0.5–1.0 V (vs. $Li^+$/Li) at current densities of 0.5, 1.0 and 2.0 mA $cm^{-2}$ with a fixed capacity of 1.0 mA h $cm^{-2}$ by using a LAND galvanostatic measurement device. For the SDSEI-Cu@Li//S cell, Li pre-deposited on the Cu substrate with the SDSEI film was used as the anode, and the cathode was a CMK-3/S composite on an Al foil current collector. The CMK-3/S composite was prepared using a melt-diffusion strategy [23]. CMK-3 and S were ground together in a weight ratio of 1:3, and heated to about 155 °C for 12 h. A homogeneous sulfur-containing slurry (≈80 wt% CMK-3/S as active material, ≈10 wt% carbon black as a conductive agent, and ≈10 wt% PVDF as binder dissolved in the *N*-methyl-2--pyrrolidone) was then spread on the Al foil by a doctor blade. The average mass loading of S in the cathode electrode was 1.2 mg $cm^{-2}$. Before testing, the bare Cu substrate or Cu substrate with the SDSEI film was pre-deposited with Li at 0.5 mA $cm^{-2}$ for 4 h, and then used as the anode of the Li–S cells. Celgard 2500 polypropylene membranes were used as the separator for both Li | Cu cells and Li–S cells. 30 μL liquid electrolyte (1.0 M LiTFSI in 1, 3-dioxolane (DOL) and 1, 2-dimethoxyethane (DME) (1:1 by volume) with 0.05 M $LiNO_3$ additive) was used for the coin cells. Galvanostatic charge/discharge cycles were conducted in the voltage range 1.7–2.8 V (vs. $Li^+$/Li). EIS measurements were performed in the frequency range $10^6$–$10^{-1}$ Hz with a voltage amplitude of 10 mV by using a VSP-300 multichannel workstation at room temperature. The EIS datas were fitted using ZView software.

### 2.4. Materials characterization

The Li deposited on the Cu substrate was protected by an Ar atmosphere in a home-made container to avoid contact with air during the transfer process before characterization. The morphologies of the samples were characterized by SEM (FEI Nova Nano-SEM 430, 10 kV). To produce TEM samples, the bare Cu substrate was cut into a 3 mm diameter disk followed by ion milling with a Gatan PIPS. The Cu disk was annealed in the same way as the working electrode in a three-electrode cell. The Cu disk with the SDSEI film was prepared for TEM, HRTEM and STEM mapping (Tecnai F20 or F30). XPS analysis was performed using an ESCALAB 250 instrument with Al Kα radiation (15 kV, 150 W) under a pressure of $4 \times 10^{-8}$ Pa. A time-of-flight secondary ion mass spectrometer (TOF-SIMS 5, ION-TOF) at a pressure below $10^{-9}$ Torr was used to analyse the chemical composition of the SDSEI film. A $Bi^{3+}$ (30 keV, 1.2 pA) ion beam was used as the primary source for detecting the composition of the sample. Sputtering with a $Cs^+$ ion beam (1 keV, 0.36 nA) was used for depth profile analysis. The sputtering time was 100s with a sputtering area of $100 \times 100$ $\mu m^2$. The sputtering rate by the $Cs^+$ beam was estimated to be 0.34 nm $s^{-1}$ [24]. Raman spectroscopy was performed using a Jobin Yvon Lab RAM HR800 with a 632.8 nm He–Ne laser, with a laser spot size of ≈1 μm. For the Raman spectroscopy sample, a commercial Cu foil was immersed in a freshly prepared 12% $HNO_3$ solution for 3 min. A sponge-type surface with a high degree of roughness was created to enhance the signal [25].

## 3. Results and discussion

The electrolyte concentration is a crucial parameter that affects the

interfacial electrochemical process on the electrode surface [26]. Recently, the emerged concept of water-in-salt electrolyte has been used to expand the electrochemical window of LIBs [27]. At room temperature, the maximum solubility of universal LiTFSI salt in water is about 21 M. At concentrations of LiTFSI above 20 M, the reduction potential of $TFSI^-$ is altered by its interaction with $Li^+$. Aggregates such as $Li_2TFSI(H_2O)_x$ become unstable below 2.9 V (vs. $Li^+/Li$), which is higher than the reduction potentials of 1.4 V for isolated $TFSI^-$ and 2.63 V for hydrogen (both vs. $Li^+/Li$). In such an electrolyte, a dense SEI film dominated with LiF is formed as a result of reduction of the $TFSI^-$ by the $Li^+$ solvation sheath, which prevents further sub-reactions [28].

Using this concept, we reported an electroreduction route to construct an artificial inorganic-rich SEI film derived from reduced salt anions on Cu substrate (Fig. 1). In a typical three-electrode cell (Fig. S1), a Cu foil as the working electrode was immersed in the water-in-salt electrolyte, and cyclic voltammetry scans were then performed in the range 1.9–3.2 V (vs. $Li^+/Li$) with a scan rate of 10 mV $s^{-1}$ for 100 cycles (the experimental details are available in Materials and methods).

After pre-processing, the flat Cu foil was covered by a dense interphase with a large number of nanoparticles (Fig. 2a and b). More importantly, the cross-view SEI image of the Cu with the SDSEI film showed that a thin film composed of nanoparticles covered on Cu surface (Figs. S2b–c), which were composed of F, O and S elements (Figs. S2d–f). A transmission electron microscopy (TEM) image clearly showed that the Cu substrate was decorated by nanoparticles of few to tens of nanometers size (Fig. 2c and Fig. S3). High-resolution TEM images of the SDSEI film showed the crystal lattice of the nanoparticles, corresponding to inorganic products LiF and $Li_2S$ (Fig. 2d). Energy-dispersive X-ray spectroscopy (EDS) analysis also demonstrated that F, S, O and C were evenly distributed on the Cu substrate (Fig. 2e–i).

To probe the chemical composition of the SDSEI film on the Cu substrate, X-ray photoelectron spectroscopy (XPS) was carried out. The surface of bare Cu using Li | Cu half cells in 1 M LiTFSI DOL/DME (0.05 M $LiNO_3$) electrolytes after 5 cycles was also characterized by XPS. The strong signal detected in the C 1s spectrum between 288.0 and 289.5 eV can be assigned to $Li_2CO_3$ or -$CSO_x$ species (Fig. 3a) [29]. The S 2p spectrum peaks detected at 162.0, 166.8, 168.0 and 169.9 eV corresponded to $Li_2S$, $Li_2S_2O_4$, $Li_2SO_3$ and –$SO_2CF_3$ (Fig. 3b), respectively [30–32]. The inorganic species $Li_2S_xO_y$ ($Li_2SO_3$, $Li_2S_2O_4$ and $Li_2S$) accounts for 89.2% but 10.8% for the organic species according to the peak area. In contrast, the solvent-derived solid electrolyte interphase on bare Cu is principally composed of organic –$SO_2CF_3$ species (almost 100%). For the O 1s spectrum (Fig. 3c), inorganic species ($Li_2SO_3$, $Li_2S_2O_4$ and $Li_2CO_3$) in SDSEI accounts for 85% based on the peak area (Fig. 3c) [33]. The detected signals of F were mainly from two species: a few fluorine organic anions (-$CF_x$) at ≈688.6 eV originating from partially reduced fragments, and dominant LiF at ≈684.7 eV (Fig. 3d) [34,35]. The proportion of LiF in the SDSEI film (72.9%) accounts more than the solvent-derived SEI film on bare Cu (19.8%) based on the ratio of peak area. Here, C, O, F and S are considered as the main species in the SEI film and normalization processing is carried out. As the Table S1 shows, the ratio of inorganic species in the salt-derived SEI film (51.88%, atomic ratio) is far greater than that in the solvent-derived SEI film (8.52%, atomic ratio). Therefore, we conclude that the SDSEI film is rich in inorganic components (mainly $Li_2S_xO_y$ and LiF) than the solvent-derived SEI film. As previous reports, on one hand, LiF is a good electrical insulator (≈$10^{-31}$ S $cm^{-1}$) to prevent electrons from crossing the SEI film [36]. On the other hand, LiF has been demonstrated to greatly suppress dendritic Li growth due to its high surface diffusivity for $Li^+$ [37]. None of the inorganic products was a decomposition product of residual salts caused by X-ray radiation (Fig. S4). Therefore, the SDSEI film is principally composed of inorganic $Li_2S_xO_y$ and LiF species, accompanied by a small amount of organic -$CF_x$. The chemical composition of the SDSEI film was also investigated using time-of-flight secondary ion mass spectrometry (TOF-SIMS) in both negative and positive modes. Several negative species were detected (Fig. 3e), including $F^-$ ($m/e = 19$), $S^-$ ($m/e = 32$), $O^-$ ($m/e = 16$) and $OH^-$ ($m/e = 17$). In particular, the signal from $F^-$ species was much stronger than from other species, which illustrated the high content of fluoride in the SDSEI film. The positive mode of TOF-SIMS was also measured under the same conditions and a positive cluster specie $(Li_2F)^+$ ($m/e = 33$) was observed (Fig. 3f). To estimate the thickness of the SDSEI film, we conducted 100s $Cs^+$ sputtering to obtain a depth profile (Fig. S5). As the sputtering time increased, the signal of the detected species all went down. Given that F and S represented the components of the SDSEI film, their declining trend suggested that the average thickness of the film was ≈14 nm (t = 41 s and sputtering rate = 0.34 nm $s^{-1}$).

The electrochemical pre-processing was performed under air atmosphere. To exclude the interference of gases (like $CO_2$), we performed control experiments under an Ar atmosphere. Similar to the results under air, a series of inorganic products, such as LiF, $Li_2O$, $Li_3N$, $Li_2S$, $Li_2S_xO_y$, were generated (Fig. S4), the main difference being the absence of $Li_2CO_3$ under Ar atmosphere. Surface-enhanced Raman spectra for the SDSEI film also confirmed that the $Li_2CO_3$ generated was associated with $CO_2$ (Fig. S6). Meanwhile, active species in Raman spectra, such as $Li_2SO_3$ centered near 935 $cm^{-1}$ and $Li_2S_2O_4$ at 1008 $cm^{-1}$ were detected. This result is consistent with the XPS results. Detailed analyses are given in the Supporting Information.

Combining the above results and analyses, the SDSEI film on the Cu substrate was generated by the electrochemical pre-processing and consisted of reductive decomposition products of the $TFSI^-$. Whether annealed under Ar or air atmospheres, the main reduced products of LiTFSI are LiF and $Li_2S_xO_y$, accompanied by a small amount of -$CF_x$. The formation mechanisms of the SDSEI film are as follows:

$$LiN(SO_2CF_3)_2 + ne^- + nLi^+ \rightarrow LiF + Li_3N + Li_2S_2O_4 + Li_{n\text{-}5}C_2F_5 \quad (1)$$

$$LiN(SO_2CF_3)_2 + e^- + Li^+ \rightarrow LiNSO_2CF_3 + LiSO_2CF_3 \quad (2)$$

$$Li_2S_2O_4 + 4e^- + 4Li^+ \rightarrow Li_2SO_3 + Li_2S + Li_2O \quad (3)$$

$$Li_2O + CO_2 \rightarrow Li_2CO_3 \quad (4)$$

The SDSEI film obtained by electrochemical processing is distinct from the conventional SEI film formed in a nonaqueous electrolyte (Fig. 1). The conventional passivated SEI film is principally composed of solvent-derived organic species like ROLi. $Li^+$ move sluggishly through the organic species by pore diffusion, which produces a low ionic conductivity and an uneven charge distribution [38]. The non-uniform $Li^+$ flux and local high concentrations of $Li^+$ accelerate the growth of Li dendrites and consumption of the electrolyte. Rather than a highly resistive layer, this new SDSEI film is largely inorganic (mainly $Li_2S_xO_y$ and LiF) with a small number of fluorine organic anions (-$CF_x$). $Li_2S_xO_y$,

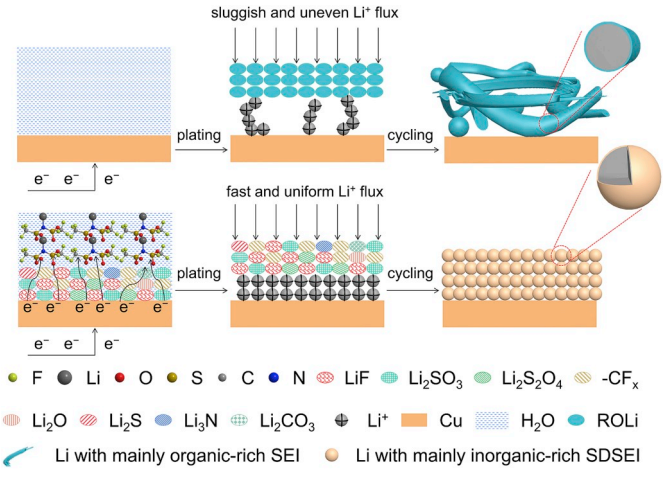


**Fig. 1.** Schematics of the Li plating behavior on different substrates.

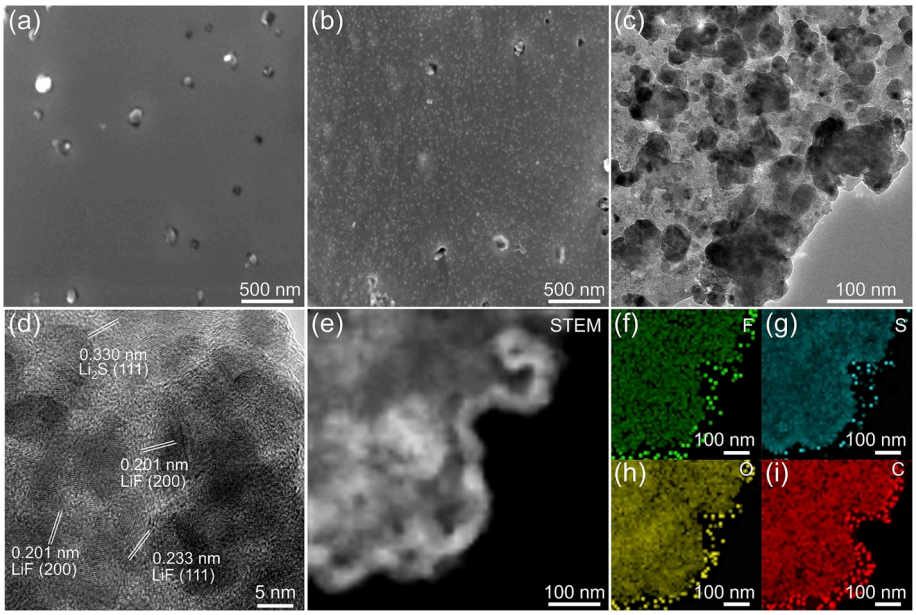


**Fig. 2.** Morphology and structure characterization. SEM images of (a) the bare Cu substrate, (b) the Cu substrate with the SDSEI film. (c) TEM image, (d) HRTEM image, and (e) STEM image of the Cu substrate with the SDSEI film and the corresponding elemental maps of (f) fluorine, (g) sulfur, (h) oxygen and (i) carbon.

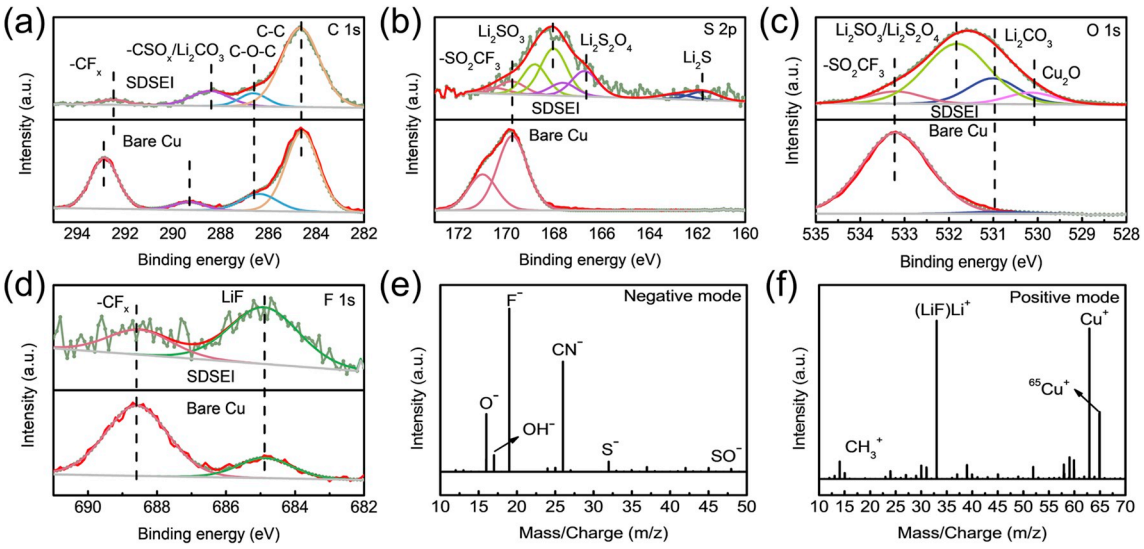


**Fig. 3.** XPS and TOF-SIMS spectra of the Cu substrate with the SDSEI film. XPS of the Cu substrate with the SDSEI film and the bare Cu with the solvent-derived SEI film: (a) C 1s spectrum, (b) S 2p spectrum, (c) O 1s spectrum, (d) F 1s spectrum. TOF-SIMS spectra of the Cu substrate with the SDSEI film: (e) Negative mode and (f) Positive mode.

provide superior ionic conductivity and fast $Li^+$ diffusion [24,39]. The abundance of LiF, with a high surface energy, produces a small interfacial resistance and uniform spatial distribution of $Li^+$, also suppressing dendritic Li growth [40]. In addition, the -$CF_x$ species inhibit space charge accumulation, which induces a homogeneous $Li^+$ distribution and facilitates homogeneous Li deposition [41,42]. As the plating process proceeds, the SDSEI film facilitates the fast and uniform deposition of spherical Li particles, resulting in a stable cycling performance.

The Li plating behavior on the Cu substrate with the SDSEI film was evaluated in a coin cell (bare Cu substrate was the controlled experiment). The amount of Li deposition was fixed at 1.0 mA h $cm^{-2}$. The deposition morphologies of Li at 1.0 and 2.0 mA $cm^{-2}$ were investigated. At a current density of 1.0 mA $cm^{-2}$, island-like Li was loosely grown on the surface of the bare Cu substrate (Fig. 4a). However, a typical rod-shaped Li dendrite appeared. During Li plating, local Li concentrations due to the high current density resulted in irregularly shaped Li deposited. The situation became more serious as the current density increased to 2.0 mA $cm^{-2}$ (Fig. 4b). This result is mainly ascribed to the low $Li^+$ conductivity and uneven $Li^+$ flux of the conventional SEI film formed from the organic solvent. Instead of typical rod-shaped dendrites, Li grown on the Cu substrate with the SDSEI film showed a smooth, spherical morphology at current densities of both 1.0 and 2.0 mA $cm^{-2}$ (Fig. 4c and d). This uniform nucleation was closely associated with the regulation of the SDSEI film, which facilitated $Li^+$ transport and produce a uniform spatial distribution of $Li^+$ for suppressing dendritic Li growth.

The overpotential of Li plating on bare Cu and the Cu substrate with the SDSEI film was investigated. In the first plating curve (Fig. 5a), a sharp voltage dropped to −128 mV (vs. $Li^+$/Li) was recorded at the beginning of the Li plating process on the bare Cu substrate, which was related to the nucleation of metallic Li. After nucleation, the voltage

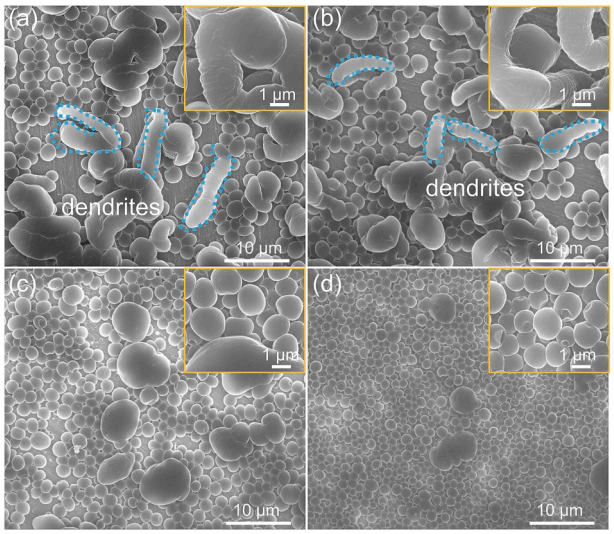


**Fig. 4.** Morphologies of the 1st Li nuclei on bare Cu substrate and the Cu substrate with SDSEI film. SEM images of Li nuclei on the bare Cu substrate at (a) 1.0 and (b) 2.0 mA cm$^{-2}$. SEM images of Li nuclei on the Cu substrate with the SDSEI film at (c) 1.0 and (d) 2.0 mA cm$^{-2}$. The insets are high-magnification SEM images of the Li nuclei.

rised to a relatively stable voltage plateau at −57 mV (vs. Li$^+$/Li), which was the mass-transfer-controlled overpotential [20]. The nucleation overpotential is defined as the difference between the minimum voltage and the later stable mass-transfer-controlled overpotential [43], which was 71 mV for a bare Cu substrate. In contrast, the curve of the Cu substrate with the SDSEI film had a much smaller voltage minimum of −82 mV (vs. Li$^+$/Li) at the nucleation stage, with a nucleation overpotential of only 54 mV. The mass-transfer overpotential depends on the applied current density and the migration properties of the Li$^+$. At the same current density of 0.5 mA cm$^{-2}$, the Cu substrate with the SDSEI film had a smaller mass-transfer overpotential of 28 mV compared to 57 mV for bare Cu. The lower mass-transfer controlled overpotential indicated that the SDSEI film effectively improved Li electrodeposition kinetics [44]. Electrochemical impedance spectroscopy (EIS) analysis of the cells was conducted to illustrate the kinetic behavior of the anodes (Fig. 5b). Both Nyquist plots had a semicircle in high frequency region, which was ascribed to Li$^+$ migration through the SEI film on the electrode surface [45]. If the average thickness of SEI film is about 14 nm (Fig. S5), a high Li$^+$ conductivity ($3.7 \times 10^{-8}$ S cm$^{-1}$) is achieved by the SDSEI film, around two times higher than bare Cu ($1.9 \times 10^{-8}$ S cm$^{-1}$). The good conductivity of Li$^+$ migration through the SDSEI film confirmes a fast Li$^+$ transport kinetics.

To further investigate the reliability of the Cu substrate with the SDSEI film, the CE of Li plating/stripping was analyzed in Li | Cu cells with 1.0 mA h cm$^{-2}$ of pre-deposited Li. The cut-off voltage of recharge was fixed at 1.0 V (vs. Li$^+$/Li). The electrochemical performance of different thickness of SDSEI films on Cu substrate was evaluated (Fig. S7). As the increasing number of pretreatment, the thickness of the SDSEI film finally reach to a maximum (≈14 nm) when the film is too thick to transport electrons (Fig. S7f). In accordance with the thickness of the SDSEI film, the initial CE was increased from 84.7% to 96.3% (higher than the bare Cu: 94.9%). The CE for the Cu substrate with the SDSEI film (14 nm) quickly increased to 98.2% after several cycles and remained stable for 140 cycles (Fig. 5c). The high CE can be attributed to the SDSEI film which effectively reduces side reactions between the deposited Li and the electrolyte. After increasing the current density to 1.0 mA cm$^{-2}$ (Fig. S8a), the initial CE of the Cu substrate with the SDSEI film exhibited 95.1%, which exceeded the Cu substrate 90.3%. And then the CE increased to a high average CE (97.8%) over 100 cycles without failure. Even at a high current density of 2.0 mA cm$^{-2}$ (Fig. S8b), the Li plating/stripping was stable without fluctuation. However, cells with the bare Cu substrate showed a rapid loss of performance after 50 cycles at 0.5 mA cm$^{-2}$ and 40 cycles at 1.0 mA cm$^{-2}$. To observe the Li deposition morphologies, we disassembled the Li | Cu cells after 40 cycles. A large number of Li dendrites with sharp tips had formed at different current densities (Fig. 5d and Fig. S9). For irregular and random Li growth, increased contact area with the nonaqueous electrolyte further consumed active Li metal and electrolyte, producing a low CE. As a comparison, the plated Li with SDSEI film became larger and thicker while maintaining the spherical morphology of the Li even after 40 plating/stripping cycles (Fig. 5e and Fig. S10). These different results confirm that the SDSEI film produces uniform Li deposition without Li dendrites.

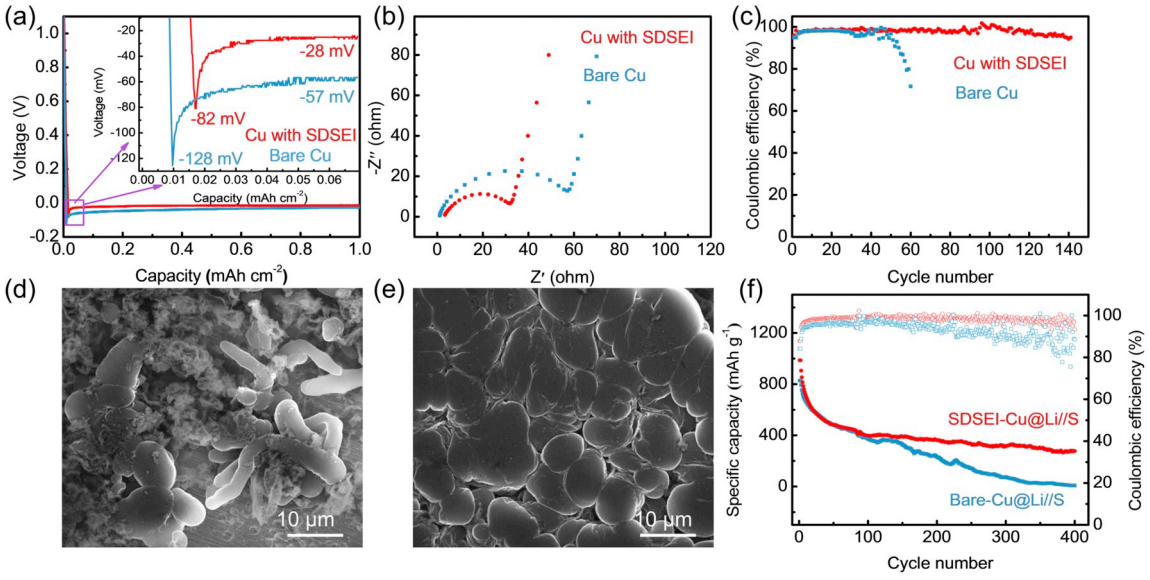


**Fig. 5.** Electrochemical performance of Li | Cu cells. (a) Voltage-time curves after the 1st Li nucleation at 0.5 mA cm$^{-2}$. (b) EIS of Li | Cu cells after the 1st cycle. (c) CE of Li deposited on bare Cu substrate and the Cu substrate with the SDSEI film at 0.5 mA cm$^{-2}$. The cells were tested with a fixed areal capacity of 1.0 mA h cm$^{-2}$. (d) SEM image of the Li morphology on the bare Cu substrate and (e) the Cu substrate with the SDSEI film. (f) Electrochemical performance of SDSEI-Cu@Li//S and Bare-Cu@Li//S cells.

Li–S full cells were assembled to verify the advantages of the above strategy for practical use with 2.0 mA h $cm^{-2}$ of pre-deposited Li. Li–S cells based on the Cu substrate with the SDSEI film and the bare Cu substrate are denoted SDSEI-Cu@Li//S and Bare-Cu@Li//S, respectively. The Bare-Cu@Li//S cell exhibited a CE about 98.1% in the first 200 cycles (Fig. 5f). However, beyond 200 cycles, it quickly dropped to 95.0%, accompanied by a fast capacity decay. After 340 cycles, the specific capacity of the cell had dropped to nearly zero. In contrast, the SDSEI-Cu@Li//S cell retained a stable CE of 99.1% over 400 cycles. The EIS of the Li–S cells were also recorded and summarized in Fig. S11 and Table S2. After the first cycle, the interfacial resistance of the SDSEI-Cu@Li//S cell (27.3 Ω) was smaller than that of Bare-Cu@Li//S (75.2 Ω), which implied that the SDSEI film had a low $Li^+$ interfacial resistance. Despite a decrease during the first 100 cycles, the interfacial resistance of the SDSEI-Cu@Li//S cell remained smaller than that of the Bare-Cu@Li//S cell. Moreover, the start of the formation of a semicircle at mid-frequency indicated the formation of a porous and thick dead Li layer [46,47]. The resistance of this dead layer in the SDSEI-Cu@Li//S cell was only 7.4 Ω compared with 12.4 Ω for the Bare-Cu@Li//S cell. This result shows that the SDSEI film effectively reduces side reactions between Li and the electrolyte, which is in good agreement with the high CE performance (Fig. 5c, and Fig. S8).

## 4. Conclusion

We have formed a SDSEI film which is mostly inorganic on a copper substrate by electroreduction pre-processing in a water-in-salt electrolyte of LiTFSI to regulate Li plating/stripping. The inorganic components (mainly $Li_2S_xO_y$ and LiF) dominate the SDSEI film and reduce the overpotential and facilitate fast $Li^+$ transport. In addition, a small number of reduced fluorine organic anions (-$CF_x$) induce a uniform space charge distribution that contributes to homogeneous Li deposition. Different from the behavior of Li deposition with a highly resistive layer composed principally of solvent-derived organic ROLi species, uniform spherical Li particles were deposited and a high CE (average 98.2%) were produced on the Cu substrate with the SDSEI film. This work provides a unique strategy to enlarge the functions of the Li salt decompositions on the protection of Li metal anode and deepen the understanding of the Li salt in the function of the SEI film.

## Acknowledgements

We thank Prof. Jun Tan for operating the SEM and valuable discussions. The authors acknowledge financial support from National Natural Science Foundation of China (Nos. 51525206 and 51521091), China; MOST (Nos. 2016YFA0200100 and 2016YFB0100100), China; Strategic Priority Research Program of the Chinese Academy of Sciences (No. XDA22010602), China; Youth Innovation Promotion Association of the Chinese Academy of Sciences (No. 2015150), China; Key Research Program of the Chinese Academy of Sciences (Grant No. KGZD-EW-T06), China; CAS-SAFEA International Partnership Program for Creative Research Teams, China.

## Appendix A. Supplementary data

Supplementary data to this article can be found online at https://doi.org/10.1016/j.jpowsour.2019.227073.

## References

[1] J.M. Tarascon, M. Armand, Nature 414 (2001) 359–367.
[2] D.C. Lin, Y.Y. Liu, Y. Cui, Nat. Nanotechnol. 12 (2017) 194–206.
[3] X.L. Xu, S.J. Wang, H. Wang, C. Hu, Y. Jin, J.B. Liu, H. Yan, J. Energy Chem. 27 (2018) 513–527.
[4] X.B. Cheng, R. Zhang, C.Z. Zhao, Q. Zhang, Chem. Rev. 117 (2017) 10403–10473.
[5] D. Aurbach, E. Zinigrad, Y. Cohen, H. Teller, Solid State Ion. 148 (2002) 405–416.
[6] H. Lee, X.D. Ren, C.J. Niu, L. Yu, M.H. Engelhard, I. Cho, M.H. Ryou, H.S. Jin, H. T. Kim, J. Liu, W. Xu, J.G. Zhang, Adv. Funct. Mater. 27 (2017), 1704391.
[7] D. Aurbach, Y. Talyosef, B. Markovsky, E. Markevich, E. Zinigrad, L. Asraf, J. S. Gnanaraj, H.J. Kim, Electrochim. Acta 50 (2004) 247–254.
[8] W. Xu, J.L. Wang, F. Ding, X.L. Chen, E. Nasybulin, Y.H. Zhang, J.G. Zhang, Energy Environ. Sci. 7 (2014) 513–537.
[9] X.B. Cheng, R. Zhang, C.Z. Zhao, F. Wei, J.G. Zhang, Q. Zhang, Adv. Sci. 3 (2016), 1500213.
[10] S.Q. Shi, P. Lu, Z.Y. Liu, Y. Qi, L.G. Hector, H. Li, S.J. Harris, J. Am. Chem. Soc. 134 (2012) 15476–15487.
[11] H. Buqa, R.I.R. Blyth, P. Golob, B. Evers, I. Schneider, M.V.S. Alvarez, F. Hofer, F. P. Netzer, M.G. Ramsey, M. Winter, Ionics 6 (2000) 172–179.
[12] Y.Y. Liu, D.C. Lin, P.Y. Yuen, K. Liu, J. Xie, R.H. Dauskardt, Y. Cui, Adv. Mater. 29 (2017), 1605531.
[13] L.M. Suo, W.J. Xue, M. Gobet, S.G. Greenbaum, C. Wang, Y.M. Chen, W.L. Yang, Y. X. Li, J. Li, Proc. Natl. Acad. Sci. 115 (2018) 1156.
[14] X.L. Fan, L. Chen, O. Borodin, X. Ji, J. Chen, S. Hou, T. Deng, J. Zheng, C.Y. Yang, S.C. Liou, K. Amine, K. Xu, C.S. Wang, Nat. Nanotechnol. 13 (2018) 715–722.
[15] B. Tong, J.W. Wang, Z.J. Liu, L. Ma, P. Wang, W.F. Feng, Z.Q. Peng, Z.B. Zhou, J. Power Sources 400 (2018) 225–231.
[16] X.B. Cheng, M.Q. Zhao, C. Chen, A. Pentecost, K. Maleski, T. Mathis, X.Q. Zhang, Q. Zhang, J.J. Jiang, Y. Gogotsi, Nat. Commun. 8 (2017) 336.
[17] L. Yu, S. Chen, H. Lee, L. Zhang, M.H. Engelhard, Q. Li, S. Jiao, J. Liu, W. Xu, J.-G. Zhang, ACS Energy Lett. 3 (2018) 2059–2067.
[18] C. Zhang, W. Lv, G.M. Zhou, Z.J. Huang, Y.B. Zhang, R.Y. Lyu, H.L. Wu, Q.B. Yun, F.Y. Kang, Q.H. Yang, Adv. Energy Mater. 12 (2018), 1703404.
[19] F. Shen, F. Zhang, Y.J. Zheng, Z.Y. Fan, Z.H. Li, Z.T. Sun, Y.Y. Xuan, B. Zhao, Z. Q. Lin, X.C. Gui, X.G. Han, Y.H. Cheng, C.M. Niu, Energy Storage Mater. 13 (2018) 323–328.
[20] Y. Deng, H.M. Lu, Y. Cao, B.B. Xu, Q.S. Hong, W. Cai, W.W. Yang, J. Power Sources 412 (2019) 170–179.
[21] Q. Wang, C.K. Yang, J.J. Yang, K. Wu, L.Y. Qi, H. Tang, Z.Y. Zhang, W. Liu, H. H. Zhou, Energy Storage Mater. 15 (2018) 249–256.
[22] A.C. Kozen, C.F. Lin, O. Zhao, S.B. Lee, G.W. Rubloff, M. Noked, Chem. Mater. 29 (2017) 6298–6307.
[23] Y.Y. Lu, Z.Y. Tu, L.A. Archer, Nat. Mater. 13 (2014) 961–969.
[24] G. Xue, J. Dong, M.S. Zhang, Appl. Spectrosc. 45 (1991) 756–759.
[25] K. Sodeyama, Y. Yamada, K. Aikawa, A. Yamada, Y. Tateyama, J. Phys. Chem. C 118 (2014) 14091–14097.
[26] L.M. Suo, O. Borodin, T. Gao, M. Olguin, J. Ho, X.L. Fan, C. Luo, C.S. Wang, K. Xu, Science 350 (2015) 938–943.
[27] F. Wang, L.M. Suo, Y.J. Liang, C.Y. Yang, F.D. Han, T. Gao, W. Sun, C.S. Wang, Adv. Energy Mater. 7 (2017), 1600922.
[28] S.H. Jiao, X.D. Ren, R.G. Cao, M.H. Engelhard, Y.Z. Liu, D.H. Hu, D.H. Mei, J. M. Zheng, W.G. Zhao, Q.Y. Li, N. Liu, B.D. Adams, C. Ma, J. Liu, J.G. Zhang, W. Xu, Nat. Energy 3 (2018) 739–746.
[29] M.R. Busche, T. Drossel, T. Leichtweiss, D.A. Weber, M. Falk, M. Schneider, M. L. Reich, H. Sommer, P. Adelhelm, J. Janek, Nat. Chem. 8 (2016) 426–434.
[30] C.Z. Zhao, X.B. Cheng, R. Zhang, H.J. Peng, J.Q. Huang, R. Ran, Z.H. Huang, F. Wei, Q. Zhang, Energy Storage Mater. 3 (2016) 77–84.
[31] X.B. Cheng, C. Yan, H.J. Peng, J.Q. Huang, S.T. Yang, Q. Zhang, Energy Storage Mater. 10 (2018) 199–205.
[32] L.M. Suo, D. Oh, Y.X. Lin, Z.Q. Zhuo, O. Borodin, T. Gao, F. Wang, A. Kushima, Z. Q. Wang, H.C. Kim, Y. Qi, W.L. Yang, F. Pan, J. Li, K. Xu, C.S. Wang, J. Am. Chem. Soc. 139 (2017) 18670–18680.
[33] L.M. Suo, O. Borodin, W. Sun, X.L. Fan, C.Y. Yang, F. Wang, T. Gao, Z.H. Ma, M. Schroeder, A. von Cresce, S.M. Russell, M. Armand, A. Angell, K. Xu, C.S. Wang, Angew. Chem. Int. Ed. 55 (2016) 7136–7141.
[34] F. Wang, O. Borodin, M.S. Ding, M. Gobet, J. Vatamanu, X.L. Fan, T. Gao, N. Edison, Y.J. Liang, W. Sun, S. Greenbaum, K. Xu, C.S. Wang, Joule 2 (2018) 927–937.
[35] J. Pan, Y.T. Cheng, Y. Qi, Phys. Rev. B 91 (2015), 134116.
[36] X.Q. Zhang, X. Chen, R. Xu, X.B. Cheng, H.J. Peng, R. Zhang, J.Q. Huang, Q. Zhang, Angew. Chem. Int. Ed. 56 (2017) 14207–14211.
[37] K. Xu, A. Von Cresce, U. Lee, Langmuir 26 (2010) 11538–11543.
[38] X.B. Cheng, C. Yan, X. Chen, C. Guan, J.Q. Huang, H.J. Peng, R. Zhang, S.T. Yang, Q. Zhang, Chem 2 (2017) 258–270.
[39] Y.Y. Liu, D.C. Lin, Z. Liang, J. Zhao, K. Yan, Y. Cui, Nat. Commun. 7 (2016), 10992.
[40] Z.H. Li, X.L. Li, L. Zhou, Z.C. Xiao, S.K. Zhou, X.H. Zhang, L.D. Li, L.J. Zhi, Nano Energy 49 (2018) 179–185.
[41] C.Z. Zhao, X.Q. Zhang, X.B. Cheng, R. Zhang, R. Xu, P.Y. Chen, H.J. Peng, J. Q. Huang, Q. Zhang, Proc. Natl. Acad. Sci. 114 (2017) 11069–11074.
[42] J.F. Qian, W.A. Henderson, W. Xu, P. Bhattacharya, M. Engelhard, O. Borodin, J. G. Zhang, Nat. Commun. 6 (2015) 6362.
[43] J. Pu, J.C. Li, Z.H. Shen, C.L. Zhong, J.Y. Liu, H.X. Ma, J. Zhu, H.G. Zhang, P. V. Braun, Adv. Funct. Mater. 28 (2018), 1804133.
[44] R. Zhang, X.R. Chen, X. Chen, X.B. Cheng, X.Q. Zhang, C. Yan, Q. Zhang, Angew. Chem. 129 (2017) 7872–7876.
[45] X.Q. Zhang, X.B. Cheng, X. Chen, C. Yan, Q. Zhang, Adv. Funct. Mater. 27 (2017), 1605989.
[46] X.Q. Zhang, X. Chen, X.B. Cheng, B.Q. Li, X. Shen, C. Yan, J.Q. Huang, Q. Zhang, Angew. Chem. Int. Ed. 57 (2018) 5301–5305.
[47] H.J. Peng, J.Q. Huang, X.Y. Liu, X.B. Cheng, W.T. Xu, C.Z. Zhao, F. Wei, Q. Zhang, J. Am. Chem. Soc. 139 (2017) 8458–8466.